Available online at www.sciencedirect.com
ScienceDirect
Journal of Power Sources 180 (2008) 154–161
JOURNAL OF POWER SOURCES
www.elsevier.com/locate/jpowsour

Performance enhancement of a direct borohydride fuel cell in practical running conditions

Cheolhwan Kim [a], Kyu-Jung Kim [a], Man Yeong Ha [b,*]

[a] *Digital Appliance Company Laboratory, LG Electronics, 391-2 Gaeumjeong-Dong, Changwon City, Gyeongnam 641-711, South Korea*
[b] *School of Mechanical Engineering, Pusan National University, San 30, Jangjeon-Dong, Kumjeong-Ku, Pusan 609-735, South Korea*

Received 23 October 2007; accepted 11 January 2008
Available online 2 February 2008

Abstract

To investigate the possibility of a cost-effective direct borohydride fuel cell (DBFC), the performance enhancement of a single cell is investigated under practical running conditions by adopting non-precious metal for the anode. Fluorinated Zr-based AB_2-type hydrogen storage alloy with an effective area of 100 cm^2 is selected as the anode catalyst. To minimize pressure loss from the enlarged cell size, a parallel-type anode channel is designed, then the principal reasons for performance degradation are analyzed. Single-cell performance is mainly enhanced by adopting a corrugated anode design, applying an anti-corrosion coating on the cathode channel, and controlling the fuel flow-rate and air humidity. The cell performance is estimated simply by measuring the wall temperature of the cell.

Keywords: Direct borohydride fuel cell; Corrugated anode; Galvanic corrosion; Hydrogen generation; Parallel anode channel; Performance

1. Introduction

Borohydrides are emerging as potential fuels for fuel cells because of their high capacity and cell voltage. In particular, sodium borohydride ($NaBH_4$) is stable in alkaline aqueous solutions. Because of the low electrochemical potential of the oxidation of BH_4^- and the high reactivity, it has been suggested that if the properties of $NaBH_4$ are fully utilized, the development of a high-quality fuel cell is possible [1–9]. Recently, sodium borohydride aqueous solution has become an interesting alternative liquid fuel for fuel cells [7–15] due to its many advantageous features such as high energy capacity and safety. Moreover, non-precious materials can be used to catalyze anodic reactions, so a low-cost system design is possible.

A direct borohydride fuel cell (DBFC) uses the $NaBH_4$ solution as fuel, and electricity is produced via the following reaction:

$$NaBH_4 + 2O_2 \rightarrow NaBO_2 + 2H_2O \quad E^\circ = 1.64\,V \qquad (1)$$

Lee et al. [1] proposed a fuel cell comprised of an aqueous alkaline solution of electrolytes containing a hydrogen-releasing agent, and achieved a discharge capacity of 6000 mAh g^{-1} of $NaBH_4$. Amendola et al. [2,3] suggested that boron redox species can provide electrochemical cells for battery or energy-storage systems. Liu et al. [8] measured the anodic performance of alkali borohydrides on several electrocatalysts to develop suitable electrode materials for borohydride-fueled fuel cells. They found the open-circuit potential to be dependent on the borohydride concentration and also to be influenced by the electrocatalyst. Liu et al. [9] also tested the electrochemical performance of a micro-borohydride fuel cell at ambient conditions, and achieved a maximum power density of 40 mW cm^{-2} using Nafion 112 membrane at room temperature. Many researchers have demonstrated the possibility of borohydrides as a fuel for fuel cells, but their operation has been mainly confined to laboratory trials. Ha et al. [18] suggested a practical design to prevent maldistribution in liquid fuel cells via simulation and experiments using full-scale samples. Recently, Li et al. [19] achieved 290 mW cm^{-2} from a direct borohydride fuel cell using a Pd mixture for the anode, and demonstrated 110 W with a five-stack cell with an effective area of 67 cm^2 when the operating temperature reached 60 °C. Kim et al. [20,21] studied the prac-

* Corresponding author. Tel.: +82 51 510 2440; fax: +82 51 512 9835.
E-mail address: myha@pusan.ac.kr (M.Y. Ha).

0378-7753/$ – see front matter © 2008 Elsevier B.V. All rights reserved.
doi:10.1016/j.jpowsour.2008.01.042

Nomenclature

$H_{air,in}$	air inlet humidity (%)
P_0	power density (mW cm^{-2})
Q_{air}	air volume flow-rate (l min^{-1})
Q_{fuel}	fuel volume flow-rate (l min^{-1})
$T_{air,in}$	air inlet temperature (°C)
$T_{fuel,in}$	fuel inlet temperature (°C)
T_{wall}	stack wall temperature (°C)

tical application of a DBFC. Recently, the effect of hydrogen generation on the cell performance was studied. This reaction not only decreases fuel utilization, but also lowers the cell performance, because hydrogen bubbles hinder ion movement in the anolyte [11,22].

In the work, reported here, the possibility of enhancing DBFC performance by adopting a non-precious metal for the anode is investigated. To obtain realistic data, experimental conditions are limited to within the practical operation conditions of the components. Through parametric analysis, critical factors to increase the performance of the DBFC are analyzed, and the results are applied in efforts to achieve this goal.

2. Experimental methodology

2.1. Experimental apparatus

A schematic representation of the experimental apparatus is shown in Fig. 1. It is divided mainly into three parts, namely: an air-supply loop, a fuel-supply loop, and a test section which includes an electric load.

The air-supply loop is an open circuit. Dry air is supplied from a high-pressure air bomb. A pressure regulator is used as a depressurizing device, and the air mass flow-rate is measured by a mass flow meter. To control air humidity, dry air passes through a bubbler which is composed of a water tank, a heater and a voltage regulator. The condensed water in the supply line, which is generated from the highly humid air, is removed by a water trap before it reaches the cathode, and its temperature and humidity are measured by a resistance temperature detector (RTD) and a humidity sensor. The regulated air is supplied to the cathode channel of a single-cell assembly, and is exhausted to the environment after reaction.

The fuel-supply loop is a closed circuit. The fuel tank is made from a 200 mm diameter acrylic tube with a length of 300 mm. It is immersed in a water bath to control the fuel temperature. A metering pump, whose discharge volume is calibrated by a precise scale, supplies a fixed volume of the fuel, the temperature of which is measured by a RTD. The regulated fuel is supplied to the anode channel and is returned to the fuel tank after reaction.

The test section consists of a single cell, a 100 W electric load, and a data-acquisition system. The single cell is connected to the electric load so as to measure its voltage and current, and the information is recorded by the data-acquisition system, which is connected to the electric load by the RS232 cable.

2.2. Test section

The configuration of the single cell is shown in Fig. 2. It consists of an anode end-plate, a nickel mesh, a membrane, and a cathode end-plate. A fluorinated Zr-based AB_2-type hydrogen storage alloy [4] was selected as the anode catalyst. It was precipitated in a nickel micro-fibre felt substrate, and was roll-pressed to form a designed shape [20,21]. A Nafion 115 membrane was used to separate the anolyte from the cathode. For the cathode, Pt 5%–C on a carbon cloth substrate was used, and a nickel mesh served as the gas-diffusion layer to separate the anode from the membrane to form a space for the fuel [12]. For the anode fuel, a solution of 10 wt.% $NaBH_4$ was prepared by dissolving sodium borohydride in 20 wt.% NaOH solution. Humidified air was supplied for the oxidant.

The end-plates were made of stainless steel and had an effective area of 100 cm^2. The aspect ratio of the end-plates was 1.56. Serpentine-shaped channels with a hydraulic diameter of 1.2 mm were formed on the cathode end-plate. The cathode end-plates are shown in Fig. 3. On the anode end-plate, parallel channels with a 2.7 mm spacing, a 0.5 mm wall thickness, and a 2 mm height were used [21].

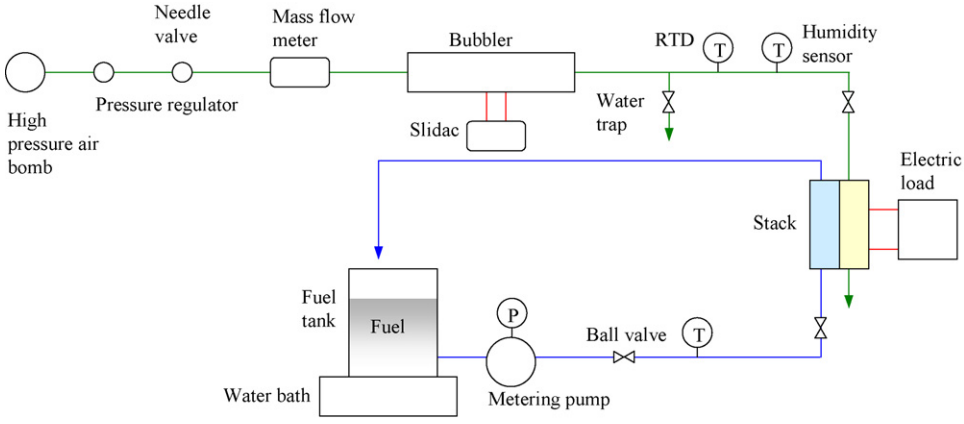

Fig. 1. Schematic representation of experimental apparatus.

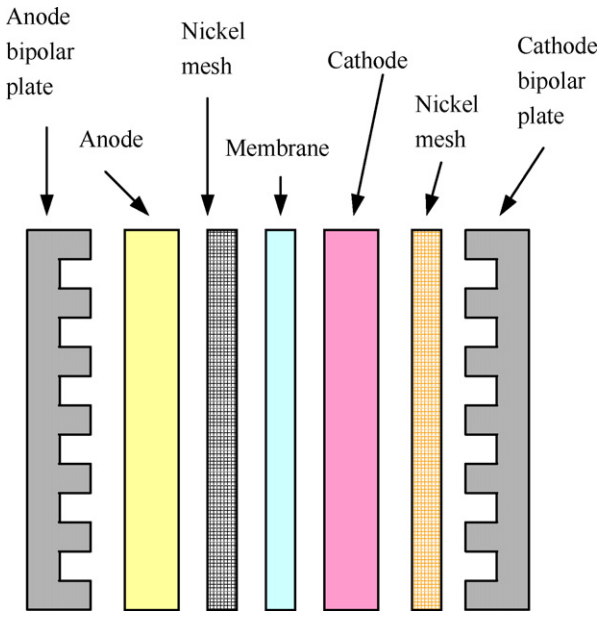

Fig. 2. Configuration of single cell.

2.3. Test method

The pressure regulator on the air-side was turned on when the target bubbler temperature was achieved, and the valve in the water trap was opened to evacuate humid air into the atmosphere. At the same time, 2 kg of fuel was prepared in the fuel tank and stored in the water bath to adjust the fuel temperature. If the fuel temperature was within the targetted values, the fuel pump was turned on to circulate the fuel in the stack. Experiment was started when air and fuel conditions meet the targetted value by closing the valve on the air-side water trap. The electric load was set in the constant-current mode, and the load was increased or decreased stepwise.

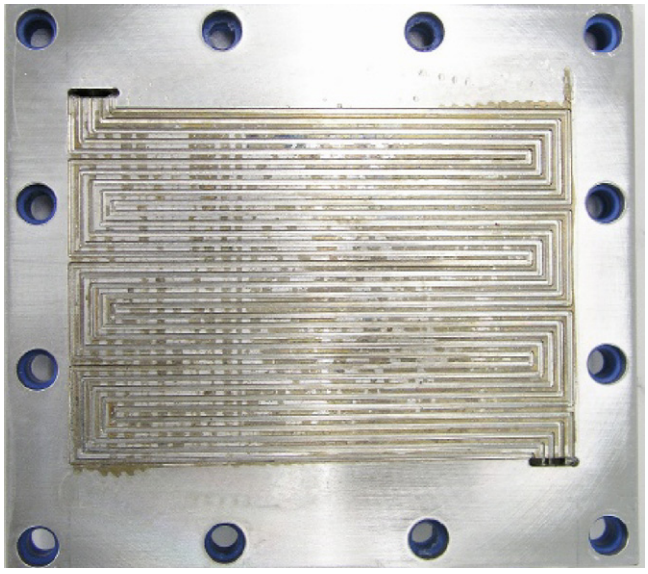

Fig. 3. Photograph of cathode end-plate.

The air inlet temperature was kept less than 70 °C for the safety of the membrane, and the fuel inlet temperature was maintained at a value less than 60 °C to suppress hydrogen generation.

3. Results and discussion

3.1. Effect of corrugated anode

One of the most important advantages of the DBFC when it is applied for portable usage is the possibility of building a cost-effective system by adopting a non-precious metal for the anode. The fuel cell system should be not only cost-effective but should also give high performance in the view of real product application. Many researchers have attempted to improve the performance of DBFCs through enhancing anode performance, and they have reported many positive results [4,19–21], yet they have used noble metals in the anode. To obtain an economical DBFC, it is necessary to maximize the performance without using noble metals in the anode. Undoubtedly, the performance of cathode should equally be optimized, but it is too early to consider the cathode because of insufficient research results.

At the same time, the size of the cell should also be practical. Recently, the results of practical sized cells have been announced [10,11]. With respect to decreasing cell size, it is necessary to consider the pressure loss problem in the anode channel, because this is one of the most important issues in the advancement of DBFCs. A serpentine channel is usually adopted for the anode. In practice, however, the serpentine channel has many disadvantages, because active hydrogen generation causes hydrogen-fuel two-phase flow, so that a large pressure loss and pressure fluctuations occur. In particular, a long and narrow serpentine channel aggravates these problems. Because it is difficult to install a large pumping device in a practical system, the fuel flow-rate should also be appropriately determined.

High-pressure loss causes another problem in the stacking of cells. Usually, it is advantageous to build cells as high as possible to obtain a higher voltage for achieving higher efficiency in the power converter, but a high-pressure loss induces maldistribution in the anode fuel which is one of the main reasons of stacking loss [23]. To reduce the loss when cells are stacked, a distribution design of the channel to reduce pressure loss is inevitable. A DBFC uses liquid fuel in the anode, and complex two-phase flow takes place in the channel from hydrogen generation [5,10,11,14,21], so severe pressure drop and pressure fluctuations in the anode channel, which will induce unstable system operation and local failure of the fuel supply, is expected.

To maximize single-cell performance without using noble metals in the anode within practical experimental conditions, a fluorinated Zr-based AB_2-type hydrogen storage alloy [4] was selected as the anode catalyst, which was precipitated into a nickel micro-fibre felt substrate. The active area of the membrane–electrode assembly (MEA) is 100 cm^2, which is derived from a 200 W power generator for portable appliances. The MEA has stainless-steel end-plates. To make a tight contact between the end-plates and the MEA, the stacking force was maintained at 980 N cm. Its performance was then measured according to the experimental conditions.

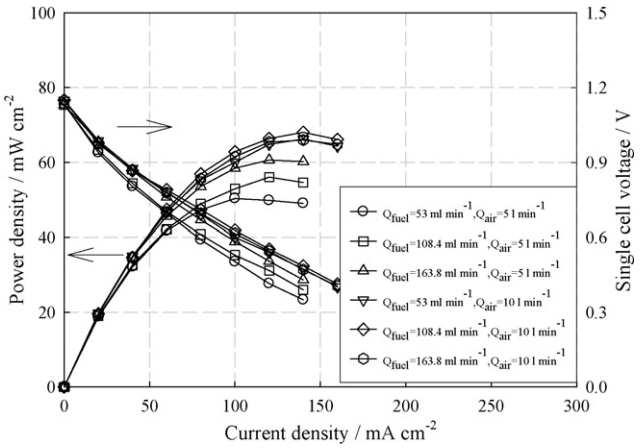

Fig. 4. Power density as a function of current density for different fuel and air flow-rates: $T_{air,in} = 40\,^{\circ}C$, $H_{air,in} = 65\%$, $T_{fuel,in} = 60\,^{\circ}C$.

Fig. 4 shows the power density as a function of current density for different flow-rates of fuel and oxidant. To obtain practical conditions, the fuel flow-rate was changed from 53×10^{-3} to $163.8 \times 10^{-3}\,l\,min^{-1}$, and the air flow-rate was changed from 5 to $10\,l\,min^{-1}$. The maximum power density is $68\,mW\,cm^{-2}$ at $140\,mA\,cm^{-2}$. Liu et al. [9] obtained $40\,mW\,cm^{-1}$ using a Ni anode. Even though the anode material is not exactly same, the cell performance is similar in both cases. Large variations in performance are observed according to the increase in air flow-rate because of the change in the partial pressure of oxygen and the cleaning effect of the high air velocity ($22\,m\,s^{-1}$ at $10\,l\,min^{-1}$). Depending on the increase in air flow-rate, NaOH generated at the cathode can be effectively removed by the driving force of the air flow, so it is beneficial to secure the active catalyst site. The difference in performance between 5 and $10\,l\,min^{-1}$ of air flow is 21% at a fuel flow-rate of $108.4 \times 10^{-3}\,l\,min^{-1}$. Increasing the fuel flow-rate has an insignificant effect on cell performance with a $10\,l\,min^{-1}$ air flow-rate, whereas the performance increases with increase in the fuel flow-rate at $5\,l\,min^{-1}$. It appears that there is an interaction between fuel flow-rate and air flow-rate, which means there is an optimum point for cell performance, but the effect of fuel flow-rate does not correspond with published data [11,16,17].

For a better understanding of the real phenomena, optical examination of the anode channel was undertaken. New end-plates were prepared from transparent acrylic material. Because the strength of acrylic is not high enough, the stacking force was reduced to a tenth of that of the stainless-steel cell. Fig. 5 shows an image of the anode channel. From the borohydride hydrolysis reaction, the borohydride electro-oxidation reaction and the hydrogen electro-oxidation reaction [10], active fuel-hydrogen two-phase flow developed in the channel. It appears that the 'slug' flow of the fuel-hydrogen blocked the fuel from contacting the anode. It is known that hydrogen generation decreases the rate of the anode reaction because hydrogen bubbles, if not removed, hinder the active sites of the catalyst [11]. In this system, the velocity of the bubbles is sufficiently rapid and they are easily removed, so that hydrogen generation is not a key determinant of cell performance.

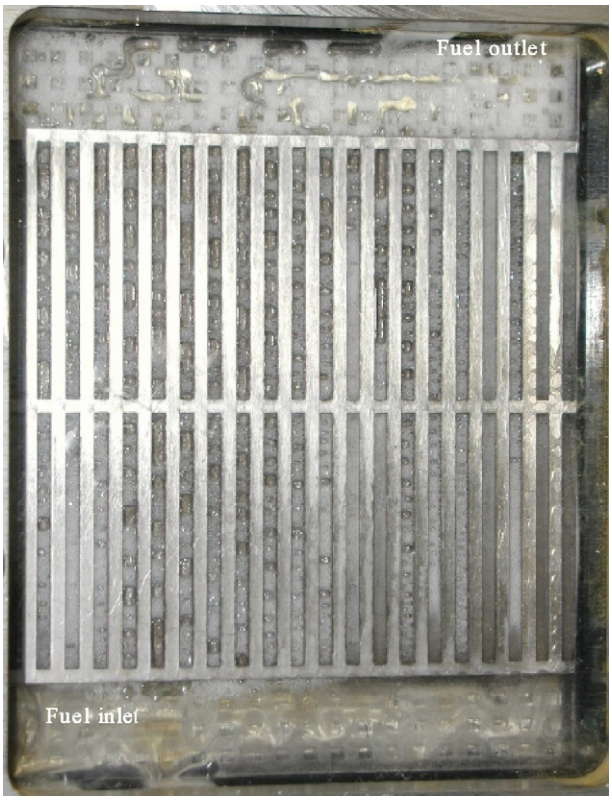

Fig. 5. Visualization photo of anode channel when active hydrogen generation occurs: $Q_{air} = 10\,l\,min^{-1}$, $T_{air,in} = 60\,^{\circ}C$, $H_{air,in} = 100\%$, $Q_{fuel} = 100 \times 10^{-3}\,l\,min^{-1}$, $T_{fuel,in} = 61\,^{\circ}C$.

To observe the real phenomena around the anode, a kit anode channel (depth: 2 mm), which can be inserted between the membrane and the anode, was prepared and subjected to optical observation, as shown in Fig. 6. In this experiment, there is a 2 mm gap between the membrane and the anode because of the presence of the kit channel. Different to the phenomena in Fig. 5, large stationary hydrogen bubbles are found between the anode and the acrylic end-plate. The hydrogen bubbles do not move even though the fuel pump is continuously operated, so it can be concluded that there are also stationary bubbles between the membrane and the anode in a normal MEA arrangement and these will form a dead zone during normal operation. Hydrogen bubbles that are held in the narrow gap between the membrane and the flat anode are not expected to be exhausted because there is no effective driving force to push them out. Because the gap is too narrow, the given pumping pressure cannot overcome the surface tension to discharge the bubbles. The stationary hydrogen acts as a resistance to smooth ion transfer from the anode to the cathode by reducing the effective area.

The cell performance slightly increases when there is a gap between the anode and the membrane and thus it is not necessary to make tight contact between these two components. Because Na^+ ions can easily be transferred through the liquid fuel, it is not necessary to attach the anode to the membrane. A more effective approach for the performance enhancement is to reduce the dead zone by evacuating the hydrogen bubbles that are held between the anode and the membrane.

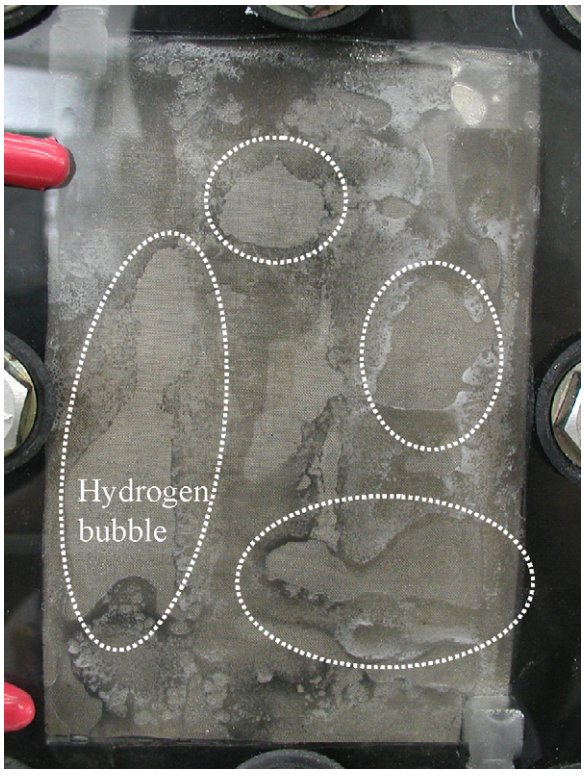

Fig. 6. Photograph of anode when hydrogen bubbles are held in narrow gap between anode and acrylic end-plate: $Q_{air} = 10\,l\,min^{-1}$, $T_{air,in} = 60\,^{\circ}C$, $H_{air,in} = 100\%$, $Q_{fuel} = 100 \times 10^{-3}\,l\,min^{-1}$, $T_{fuel,in} = 61\,^{\circ}C$.

A corrugated-shaped anode was designed to utilize the phenomena as shown in Fig. 7. The corrugated anode had a gap between the valleys, so it was expected to assist the evacuation of the hydrogen. Moreover, a better performance is anticipated than that of the conventional flat-type anode even though the contact point between the anode and the membrane is small. Power density as a function of current density for different anode shapes is shown in Fig. 8. The corrugated anode gives 27% higher performance than that from a flat anode. It is concluded that the improved performance is due to the removal of hydrogen held in the gap between the anode and the membrane so that ion transfer from the liquid fuel to the membrane becomes smoother.

Fig. 7. Photograph of corrugated anode.

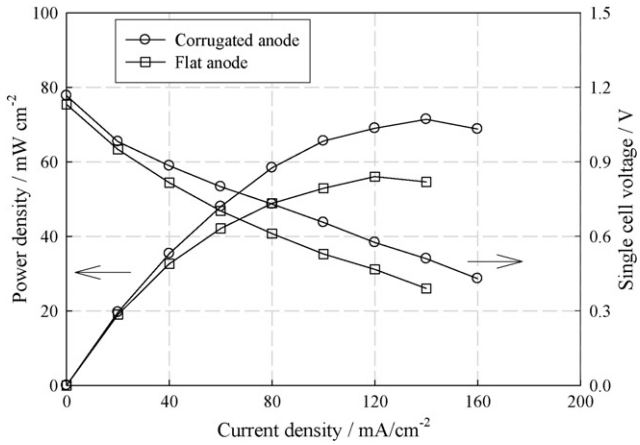

Fig. 8. Power density as a function of current density for flat and corrugated anode: $Q_{air} = 5\,l\,min^{-1}$, $T_{air,in} = 45.5\,^{\circ}C$, $H_{air,in} = 65\%$, $Q_{fuel} = 108.4 \times 10^{-3}\,l\,min^{-1}$, $T_{fuel,in} = 60\,^{\circ}C$.

3.2. Effect of galvanic corrosion

Fig. 3 shows the surface of the cathode end-plate after experiment. Although this component is made of stainless steel which has high corrosion resistance, many black spots are observed on the surface of the channel and these are electrically resistant. It appears that the stainless-steel end-plate is subject to galvanic corrosion. Accordingly, a gold anti-corrosion coating is applied to the channel surface.

Fig. 9 shows the power density as a function of current density for the anti-corrosion coated cell according to a change in air humidity. The performance is increased by 56% as a result of the anti-corrosion coating, which secures the active area for the smooth transfer of electrons. Additionally, the cell performance is increased about 11% when the humidity is raised from 65 to 85%. It is considered that humidification of the air has a positive effect on the removal of sodium hydroxide that accumulates on the surface of the cathode catalyst.

As with the end-plates, the colour of the nickel mesh, which is located between the membrane and the cathode, turned black.

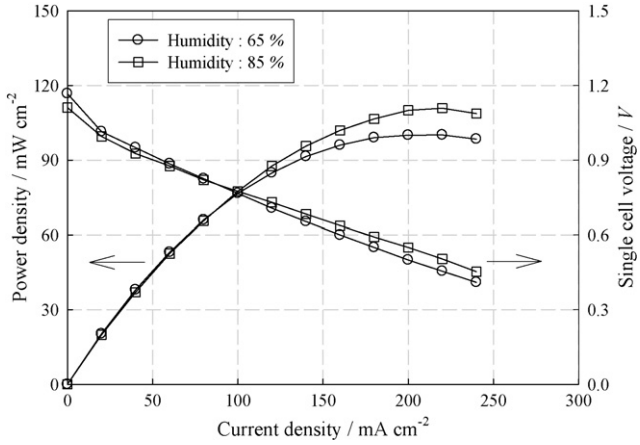

Fig. 9. Power density as a function of current density for different humidity for anti-corrosion coated cathode channel: $Q_{air} = 5\,l\,min^{-1}$, $T_{air,in} = 46\,^{\circ}C$, $Q_{fuel} = 108.4 \times 10^{-3}\,l\,min^{-1}$, $T_{fuel,in} = 60\,^{\circ}C$.

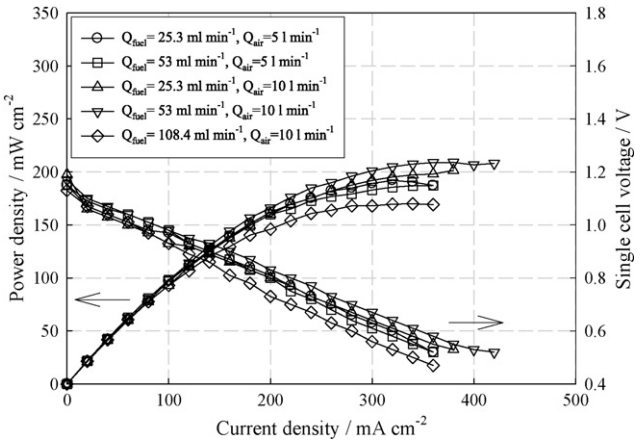

Fig. 10. Power density as a function of current density for anti-corrosion coated cathode mesh: $T_{air,in} = 59\,^{\circ}C$, $H_{air,in} = 98\%$, $T_{fuel,in} = 37\,^{\circ}C$.

Even though nickel has a higher corrosion resistance than stainless steel, its corrosion resistance is not high enough and so an anti-corrosion coating was applied to gain a performance improvement. The experimental results are presented in Fig. 10. The cell performance increases by 72% compared with the use of uncoated-nickel mesh. For an increase in the fuel flow-rate from 25.3×10^{-3} to $53 \times 10^{-3}\,l\,min^{-1}$, the performance increases by only 2.5%. It seems that the activity of anode catalyst cannot be enhanced just by increasing the fuel flow-rate; the highest cell performance is obtained at a $53 \times 10^{-3}\,l\,min^{-1}$ of fuel flow-rate and a $10\,l\,min^{-1}$ of air flow-rate. Moreover, the performance is lower than that with a $5\,l\,min^{-1}$ of air flow-rate when the fuel flow-rate is $108.4 \times 10^{-3}\,l\,min^{-1}$.

The pressure loss at the anode side changes dramatically with experimental time. The results are presented in Fig. 11. Large fluctuations occur over the whole experimental period. Moreover, a negative pressure loss is found, which indicates a back flow of fuel. Generated hydrogen rushes to the limited area of the fuel outlet, so the absolute pressure in the fuel outlet suddenly increases, and the increased pressure pushes the fuel back to the fuel inlet. This phenomenon releases the pressure load in the fuel outlet, and normal hydrogen evacuation follows. Finally, irregular pressure changes are continuously observed. The pressure loss increases up to 20 kPa, which is acceptable for a general pumping pressure, so the parallel-type anode channel is effective for a DBFC even though the characteristics of the pressure fluctuation should be enhanced.

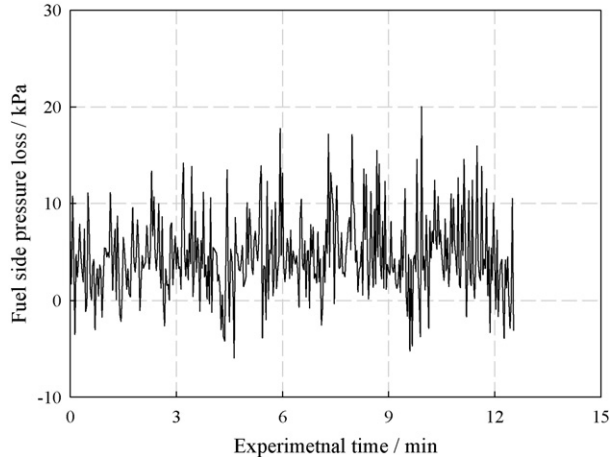

Fig. 11. Fuel side pressure loss: $Q_{air} = 10\,l\,min^{-1}$, $T_{air,in} = 46\,^{\circ}C$, $H_{air,in} = 98\%$, $Q_{fuel} = 108.4 \times 10^{-3}\,l\,min^{-1}$, $T_{fuel,in} = 60\,^{\circ}C$.

3.3. Effect of wall temperature

From the experimental analysis, it is found that the air flow-rate, humidity and fuel flow-rate are the main parameters that influence the performance of a borohydride fuel cell. Nevertheless, their effects are not very consistent. Especially, the effect of fuel flow-rate is not well matched. The reason for this inconsistency could be the absence of important factors. On the basis of low performance in the case of a high fuel flow-rate, it can be assumed that increasing of the fuel-flow-rate decreases the temperature of the MEA. Since measurement of the MEA temperature is almost impossible, wall temperatures of the cell were measured as an alternative. The MEA was tightly contacted to the end-plate, and since stainless steel has a high thermal conductivity, the MEA temperature can be estimated from the end-plate temperature. Fig. 12 shows the relation between the fuel flow-rate and the cell performance. As expected, the fuel flow-rate has a negative effect on cell performance and can be expressed by

$$P_0 = 238.6 - 1.8Q_{fuel}, \qquad r^2 = 0.58 \tag{2}$$

where r is the correlation coefficient. It can be concluded a reduction in the fuel flow-rate can enhance the cell performance. These results are different from previous studies. However, the wall temperature is positively related to cell performance under these experimental conditions, as shown in Fig. 13, and the value of r^2 is sufficiently high, i.e.,

$$P_0 = -70.5 + 3.8T_{wall}, \qquad r^2 = 0.87 \tag{3}$$

Therefore, it can be concluded that a reduced fuel flow-rate increases the MEA temperature. From the lack of a cool-

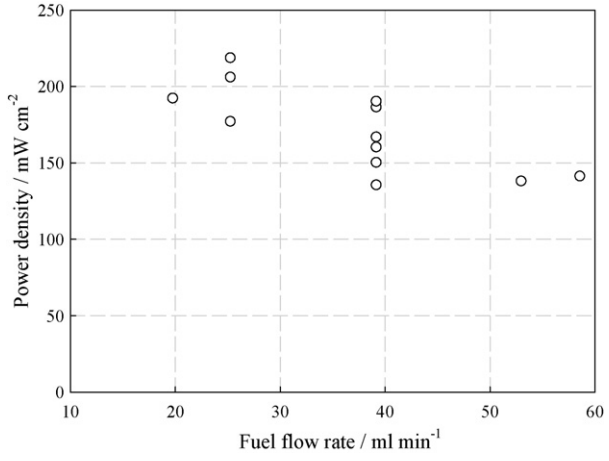

Fig. 12. Power density as a function of fuel flow-rate: $Q_{air} = 4$–$11.1\,l\,min^{-1}$, $T_{air,in} = 58.1$–$61.4\,^{\circ}C$, $H_{air,in} = 100\%$, $Q_{fuel} = 19.8$–$58.6 \times 10^{-3}\,l\,min^{-1}$, $T_{fuel,in} = 31.8$–$39.4\,^{\circ}C$.

Table 1
Experimental conditions and results

Air flow-rate ($l\,min^{-1}$)	Air inlet temperature (°C)	Fuel flow-rate ($\times10^{-3}\,l\,min^{-1}$)	Fuel inlet temperature (°C)	Stack wall temperature (°C)	Current density ($mA\,cm^{-2}$)	Power density ($mW\,cm^{-2}$)
4.0	58.1	39.2	32.2	56.9	260	135.2
5.0	58.4	25.3	22.7	67.8	340	176.8
5.0	58.9	53.0	34.5	55.5	260	137.8
7.5	59.5	19.8	31.8	70.0	320	192.0
7.5	60.3	39.2	32.6	60.1	340	166.6
7.5	60.0	39.2	34.0	62.3	300	150.0
7.5	59.9	39.2	33.0	62.4	320	160.0
7.5	59.7	39.2	37.7	60.0	320	160.0
7.5	59.3	58.6	37.6	55.6	300	141.0
10.0	60.6	25.3	32.2	73.4	420	205.8
10.0	59.9	25.3	33.6	75.5	420	218.4
11.1	60.7	39.2	39.4	61.9	380	186.2
11.0	61.4	39.2	33.7	67.7	380	190.0

ing source, heat generation in the cell becomes severe, which increases the MEA temperature leading to an enhancement in cell performance. Nevertheless, safety considerations pose a limit to which the wall temperature can be increased.

Table 1 provides a summary of the experimental conditions and results. The relationships between the factors and the cell performance are as follows:

$$P_0 = -766.2 + 15.7T_{\text{air,in}}, \qquad r^2 = 0.30 \tag{4}$$

$$P_0 = 205.6 - 1.0T_{\text{fuel,in}}, \qquad r^2 = 0.02 \tag{5}$$

$$P_0 = 104.8 + 8.5Q_{\text{air}}, \qquad r^2 = 0.52 \tag{6}$$

The effect of the air inlet temperature is not very strong, and the fuel inlet temperature is not an important factor because of the low r^2 value. The air flow-rate can be an important factor which corresponds with other published data [11,17].

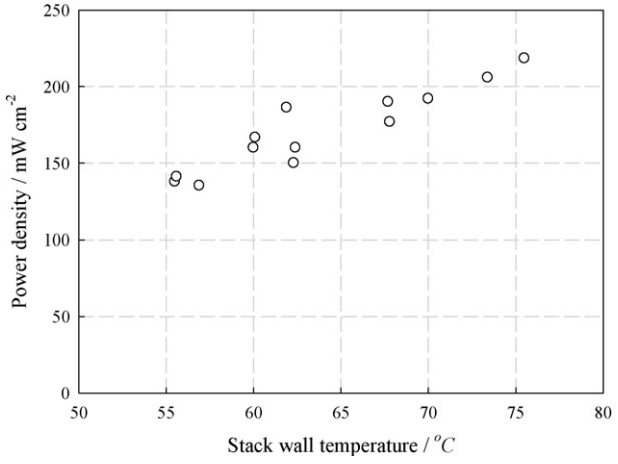

Fig. 13. Power density as a function of stack wall temperature: Q_{air} = 4–11.1 l min^{-1}, $T_{\text{air,in}}$ = 58.1–61.4 °C, $H_{\text{air,in}}$ = 100%, Q_{fuel} = 19.8–58.6 × 10^{-3} l min^{-1}, $T_{\text{fuel,in}}$ = 31.8–39.4 °C.

4. Conclusions

To investigate the possibility of a cost-effective DBFC, a non-precious metal has been used for an anode. The experimental conditions are confined within practical conditions. The performance is enhanced by adopting a corrugated anode design, applying an anti-corrosion coating in cathode channel, and controlling the fuel flow-rate and air humidity.

Stationary hydrogen bubbles which are trapped in the narrow gap between the membrane and the anode degrade DBFC performance. This problem is solved by adopting a corrugated anode design which makes a 2 mm gap between the membrane and the anode by giving valleys for effective evacuation of the hydrogen bubbles.

Galvanic corrosion is the most serious contributor to performance degradation of the DBFC. Stainless-steel end-plates and a nickel mesh for the diffusion layer are subject to attack in the highly corrosive environment. To eliminate this possibility, an anti-corrosion coating is applied, and proves effective in performance enhancement.

With increase in air humidity from 65 to 85%, cell performance is raised by about 11%. It is concluded that humidification of the air has a positive effect on the removal of sodium hydroxide that accumulates on the surface of the cathode catalyst.

Fuel flow-rate controls the wall temperature. A low fuel flow-rate increases the stack and the MEA temperatures. Due to the lack of a cooling source, heat generation in the cell from the ohmic loss becomes severe, which increases the MEA temperature and leads to an enhancement in cell performance. Performance is estimated simply by measuring the wall temperatures of the cell.

Acknowledgements

This work was supported by LG Electronics Co. The authors would like to thank Prof. Seijirau Suda, Kogakuin University, Japan for supplying fluorinated metal hydride and valuable discussions on the mechanism of the DBFC. This work was sup-

ported by the Korea Foundation for International Cooperation of Science & Technology (KICOS) through a grant provided by the Korean Ministry of Science & Technology (MOST) in K20702000013-07E0200-01310.

References

[1] J.Y. Lee, H.H. Lee, J.H. Lee, D.M. Kim, US Patent 5,599,640 (1997).
[2] S. Amendola, US Patent 5,8043,29 (1998).
[3] S. Amendola, C.P. Onnerud, M.T. Kelly, P.J. Petillo, S.L. Sharp-Goldman, M. Binder, J. Power Sources 84 (1999) 130.
[4] S. Suda, US Patent 6,358,488 B1 (2002).
[5] S.C. Amendola, S.L. Sharp-Goldman, M.S. Janjua, N.C. Spencer, M.T. Kelly, P.J. Pdtillo, M. Binder, Int. J. Hydrogen Energy 25 (2000) 969.
[6] Y. Kojima, K. Suzuki, K. Fukumoto, M. Sasaki, T. Yamamoto, Y. Kawai, H. Hayashi, Int. J. Hydrogen Energy 27 (2002) 1029.
[7] Y. Kojima, Y. Kawai, M. Kimbara, H. Nakanishi, S. Mstsumoto, Int. J. Hydrogen Energy 29 (2004) 1213.
[8] B.H. Liu, Z.P. Li, S. Suda, Electrochim. Acta 49 (2004) 3097.
[9] B.H. Liu, Z.P. Li, K. Arai, S. Suda, Electrochim. Acta 50 (2005) 3719.
[10] Z.P. Li, B.H. Liu, J.K. Zhu, S. Suda, J. Power Sources 163 (2006) 555.
[11] K.T. Park, U.H. Jung, S.U. Jeong, S.H. Kim, J. Power Sources 162 (2006) 192.
[12] J.H. Wee, J. Power Sources 161 (2006) 1.
[13] J.H. Wee, J. Power Sources 155 (2006) 329.
[14] C. Ponce de Leon, F.C. Walsh, D. Pletcher, D.J. Browning, J.B. Lakeman, J. Power Sources 155 (2006) 172.
[15] M. Chatenet, F. Micoud, I. Roche, E. Chainet, J. Vondrak, Electrochim. Acta 51 (2006) 5452.
[16] M.H. Atwan, C.L.B. Macdonald, D.O. Northwood, E.L. Gyenge, J. Power Sources 158 (2006) 36.
[17] H. Cheng, K. Scott, J. Power Sources 160 (2006) 407.
[18] M.Y. Ha, C.H. Kim, Y.W. Jung, S.G. Heo, J. Mech. Sci. Technol. 20 (6) (2006) 840.
[19] Z.P. Li, B.H. Liu, K. Arai, S. Suda, J. Alloys Compd. 404–406 (2005) 648.
[20] C.H. Kim, K.J. Kim, S.C. Ha, T.H. Cho, M.S. Park, M.H. Lee, S.T. Ko, S.G. Heo, Korea Patent 10-0486598 (2005).
[21] C.H. Kim, PhD thesis of Pusan National University, 2007, p. 46.
[22] B.H. Liu, Z.P. Li, S. Suda, J. Alloys Compd. 415 (1–2) (2006) 288.
[23] J.H. Koh, H.K. Seo, C.G. Lee, Y.S. Yoo, H.C. Lim, J. Power Sources 115 (2003) 54.